The Triple Lock: A Model of Sequential Bio-Geochemical Filters on the Path to Complex Life

Tema P. Igoshev
Independent Researcher
plca@ya.ru

Version 4.3 — February 2026

Abstract

We propose a physically motivated replacement for the speculative factors $f_l \times f_i$ in the Drake Equation. The Triple Lock Index (TLI) evaluates the probability of complex (eukaryotic) life through three sequential filters: spectral compatibility with oxygenic photosynthesis (Filter 1), a sustained phosphorus cycle via plate tectonics (Filter 2), and an oceanic habitable zone permitting eukaryogenesis under stellar radiation (Filter 3). Applied to a catalogue of 13 worlds, TLI spans five orders of magnitude—from ∼5% (Kepler-442b) to $< 10^{-5}$% (Proxima b)—identifying eight distinct failure patterns. The model correctly predicts Venus's failure mode (hydrosphere loss at Filter 2) in a blind run, generates falsifiable predictions with quantitative thresholds, and yields $N \approx 55$ civilisations in the Galaxy when integrated into the Drake Equation—consistent with the Fermi Paradox. Monte Carlo analysis (10,000 iterations) reveals that TLI uncertainty for well-characterised worlds is ∼28–38×, while for M-dwarf planets it reaches 10^4–10^7×, driven by unconstrained XUV fluxes—identifying these as priority observational targets for JWST/HWO/LIFE. Applied to the full NASA habitable-zone catalogue (6,128 confirmed exoplanets as of February 2026), TLI reduces 73–78 habitable-zone candidates to 11–13 physically promising worlds, of which only 6–7 exceed TLI > 1%—all located beyond 140 light-years. This result exposes a systematic observational selection bias: current surveys preferentially discover M-dwarf planets with low TLI, while physically promising K- and G-dwarf candidates remain underrepresented.

Contents

1 Introduction

The Drake Equation, proposed in 1961, remains the standard framework for estimating the number of technological civilisations in the Galaxy (Drake, 1961). However, two of its key factors—the probability of life (f_l) and the probability of intelligence (f_i)—lack observational constraints and vary across authors by ten or more orders of magnitude. This uncertainty effectively invalidates the result: any desired N can be obtained by choosing "convenient" values.

We propose replacing the product $f_l \times f_i$ with a physically grounded index—the Triple Lock Index (TLI)—which evaluates the probability of complex (eukaryotic) life on a given planet through three sequential filters. Each filter corresponds to an independent physical barrier identified in the literature: spectral compatibility of the host star with oxygenic photosynthesis (Burnetti et al., 2026; Hall et al., 2023), the geochemical phosphorus cycle as the ultimate limiting nutrient (Tyrrell, 1999), and the energetic threshold for a eukaryotic genome (Lane & Martin, 2010).

The key distinction between TLI and existing habitability indices (ESI, PHI) is that the model does not assess "Earth-likeness" but traces a causal chain: stellar spectrum → photosynthesis → oxygen → complex life. Each link in this chain can break for a specific, diagnosable reason.

Unlike similarity-based indices such as the Earth Similarity Index (ESI), which quantify how closely a planet's physical parameters resemble Earth's, TLI evaluates a causal process. A planet may score high on ESI yet fail TLI (e.g. a tectonically dead Earth-twin around a Sun-like star), or score low on ESI yet pass TLI (e.g. Kepler-442b, a super-Earth around a K-dwarf with TLI exceeding Earth's). This process-based approach is the principal methodological contribution of the present work. Table 1 summarises the key differences between TLI and existing frameworks.

Table 1: Comparison of major habitability assessment frameworks for complex (eukaryotic) life.

Feature	**ESI**	**PHI**	**EHI**	**TLI (this work)**
Type of approach	Similarity-based	Similarity-based	Hybrid	Causal process-based
Evaluates causal chain	No	Partial	No	Yes (full chain)
Diagnoses failure modes	No	No	No	Yes (8 patterns)
Falsifiable predictions	No	No	No	Yes
M-dwarf penalty	None	Weak	Partial	Strong & explicit
Validation beyond Earth	No	No	No	Yes (blind test on Venus)
Uncertainty quantification	Not reported	Not reported	Not reported	Monte Carlo (10 000 iter.)
Typical uncertainty range	—	—	—	28–38× (well-characterised) 10^4–10^7× (M-dwarf planets)

2 Model Architecture

The Triple Lock model expresses the probability of complex life as a product of three conditional probabilities:

$$\mathrm{TLI} = P(F_1) \times P(F_2) \times P(F_3) \times 100\% \tag{1}$$

where:

$P(F_1)$ — **Spectral Filter.** The probability that the host star's spectrum delivers sufficient photons for chlorophyll-based oxygenic photosynthesis, accounting for photoinhibition at excessive flux and competition with retinal-based systems around cool stars.

$P(F_2)$ — **Geochemical Filter.** The probability that the planet sustains a phosphorus cycle through plate tectonics and ocean–mantle contact (parameter η), sufficient to trigger and maintain the Great Oxidation Event (GOE).

$P(F_3)$ — **Radiation Filter.** The probability that an oceanic zone exists where light is sufficient for photosynthesis while UV/XUV radiation is low enough for a complex ($\sim$20,000-gene) eukaryotic genome to survive, factoring in the probability of the endosymbiotic event itself.

The filters are sequential in the sense that each addresses a necessary condition for the next: without passing F_1, F_2 cannot initiate; without F_2, F_3 is irrelevant. The multiplicative form ensures that failure at any single stage drives the overall TLI down by orders of magnitude—explaining the observed range from $\sim$5% (best candidates) to $< 10^{-5}$% (dead worlds).

Feedback loop: High XUV flux (F_3) forces photosynthesis to deeper water where light is dimmer (F_1), reducing net primary productivity and slowing oxygen accumulation (F_2). This positive feedback amplifies the suppression of complex life around active M dwarfs. A quantitative single-pass correction for this effect is developed in Appendix A.5.

3 Filter 1: Spectral Barrier

Oxygenic photosynthesis on Earth uses chlorophyll a and b, absorbing primarily in the 400–700 nm range (photosynthetically active radiation, PAR). The key question for each exoplanet is whether the host star provides sufficient PAR photons for chlorophyll to outcompete alternative pigments—primarily retinal.

Burnetti et al. (2026) demonstrated that chlorophyll and retinal create an "evolutionary priority effect": whichever pigment occupies the dominant niche first blocks transition to the other. On Earth, chlorophyll prevailed, likely due to the high PAR flux from a Sun-like star. Around M dwarfs, peak emission shifts to the near-IR, PAR fraction drops from $\sim$37% (G2V) to $\sim$1% (M8V), and retinal may gain the competitive advantage—blocking the path to oxygenic photosynthesis and, consequently, to complex life.

The concept of evolutionary priority effects as a constraint on major innovations has independent theoretical support (Stroud et al., 2024). Furthermore, Gómez-Consarnau et al. (2019) showed that microbial rhodopsins absorb as much solar energy in the modern ocean as chlorophyll-based phototrophs, confirming that retinal remains a viable competitor even on present-day Earth.

Hall et al. (2023) introduced the Photosynthetic Habitable Zone (PHZ)—the region around a star where both liquid water and oxygenic photosynthesis are possible. The PHZ is significantly narrower than the classical habitable zone for stars later than K5V.

DasSarma & Schwieterman (2018) proposed the "Purple Earth" hypothesis, suggesting that retinal-based organisms dominated the Archaean ocean before chlorophyll emerged. This supports the notion of pigment competition and justifies the "blocking factor" for cool stars in our model.

Expert estimates of $P(F_1)$ are based on three components: the PAR fraction in the stellar spectrum, a photoinhibition correction at high flux, and the retinal blocking effect for cool stars. For Sun-like stars (G2V–K1V), $P(F_1) \approx 0.70$–0.85; for early M dwarfs (M1V), $\sim$0.10–0.15; for late M dwarfs (M5V–M8V), $\sim$0.005–0.05. The full analytical formula is given in Appendix A.

4 Filter 2: Geochemical Trap

Photosynthesis requires not only light but also nutrients. Phosphorus is the ultimate limiting element for oceanic primary productivity on geological timescales (Tyrrell, 1999). Phosphorus delivery to the ocean is controlled by continental weathering, which in turn requires active plate tectonics.

Filter 2 evaluates the probability that a planet sustains a phosphorus cycle long enough ($\geq$1–2 Gyr) to trigger the Great Oxidation Event. Three key parameters govern this: tectonic activity (dependent on planetary mass), ocean–mantle contact (η—zero for Venus without an ocean or K2-18b with an ice shell), and weathering intensity.

Earth is the only known case where the GOE occurred successfully, and it took $\sim$2 Gyr after the emergence of cyanobacteria. This alone indicates that even under ideal conditions (active tectonics, full ocean–mantle contact), GOE is not guaranteed.

The value $P_{\mathrm{GOE}} = 0.40$ reflects this $\sim$2 Gyr delay between the emergence of cyanobacteria and the GOE, despite intermittent "whiffs" of oxygen (Lyons et al., 2014). Geochemical sinks (dissolved Fe^{2+}, volcanic H_2S, biogenic CH_4) suppressed net O_2 accumulation for an extended period, indicating that even under ideal conditions the GOE is not inevitable. A Poisson estimate ($\lambda = 1$ event per 2 Gyr window) yields $P \approx 0.39$, consistent with our adopted value.

Filter 2 admits three failure types: tectonic collapse (Mars—core cooled, tectonics ceased), hydrosphere loss (Venus—ocean evaporated, $\eta \to 0$), and ice isolation (K2-18b—ice shell blocks ocean–mantle contact).

Expert estimates of $P(F_2)$: Earth $\sim$0.40, Kepler-442b $\sim$0.60, Kepler-186f $\sim$0.35, Mars $\sim$0.005 (dead tectonics), Venus $\sim$0.03 ($\eta \to 0$).

5 Filter 3: Radiation Barrier

Lane & Martin (2010) showed that a eukaryotic cell with a $\sim$20,000-gene genome requires orders of magnitude more energy per gene than a prokaryotic cell. Mitochondrial endosymbiosis—the only known mechanism to overcome this barrier—occurred on Earth once in 4 billion years.

Filter 3 models a spatial trap in the ocean: at the surface, light is abundant but stellar XUV radiation is lethal to complex genomes; at depth, the genome is protected but light is too dim for photosynthesis. The habitable zone is the intermediate layer where light remains sufficient and radiation is already safe. The width of this zone (Δ_{HZ}) determines $P(F_3)$.

For Earth (G2V, XUV = 1×), the habitable zone extends from ∼7 to ∼90 m depth—a wide corridor. For TRAPPIST-1e (M8V, XUV = 50×; tidal heating models suggest partial interior warming, Barr et al. 2018), the safe depth begins below ∼46 m while light runs out at ∼36 m—the zone collapses, $\Delta_{\rm HZ} = 0$. For Proxima b (M5.5V, XUV = 250× due to superflares), the situation is worse still.

Even with a wide zone, endosymbiosis is an extremely improbable event. We account for this through a baseline endosymbiosis probability calibrated against Earth.

Expert estimates of $P(F_3)$: Earth ∼0.05, Kepler-442b ∼0.10 (low XUV, wide zone), TRAPPIST-1e $< 10^{-4}$ (zone absent), Proxima b $< 10^{-4}$.

6 Catalogue of 13 Worlds

Table 2 presents expert estimates of the three filters for 13 worlds, selected to span the full parameter range—from optimal K-dwarf hosts to demonstrably uninhabitable objects (airless worlds, icy moons, planets around ultracool dwarfs). The estimates are grounded in the physical arguments of Sections 3–5 and are reproduced by the analytical formulae of Appendix A to within a factor of 0.2–3.4× (see comparison table in Appendix A).

Table 2: Triple Lock Index for 13 worlds (expert estimates).

Object	**Sp. type**	$\boldsymbol{P(F_1)}$	$\boldsymbol{P(F_2)}$	$\boldsymbol{P(F_3)}$	**TLI, %**	**Failure pattern**
Kepler-442b	K1V	0.85	0.60	0.10	5.10	Best scenario
Earth	G2V	0.70	0.40	0.05	1.40	Passed
Kepler-452b	G2V	0.70	0.35	0.05	1.23	Age degradation
Mars (ancient)	G2V	0.70	0.005	N/A	0.35*	Tectonic collapse
LHS 1140 b	M4.5V	0.12	0.55	0.03	0.20	Spectral barrier
Kepler-186f	M1V	0.15	0.35	0.02	0.11	Spectral barrier
Venus (blind)	G2V	0.70	0.03	0.04	0.084	Hydrosphere loss
Gliese 667Cc	M1.5V	0.14	0.20	0.01	0.028	Combined barrier
Europa	G2V	0.001	0.30	0.80	0.024	No photons
Teegarden's b	M7V	0.04	0.15	0.002	0.0012	Triple suppression
TRAPPIST-1e	M8V	0.05	0.03	5×10^{-4}	7.5×10^{-5}	Triple suppression
Proxima b	M5.5V	0.05	0.04	5×10^{-5}	1×10^{-5}	Radiation trap
K2-18b	M3V	0.08	<0.001	N/A	$< 10^{-5}$	Ice isolation

*TLI for Mars computed as $P(F_1) \times P(F_2) \times 100\%$ without F_3, as life is halted at Filter 2.
For TRAPPIST-1e and Proxima b, $P(F_3)$ is set to an expert floor value reflecting parameter uncertainty; the analytical formula yields $\Delta_{\rm HZ} = 0$ for both objects (see Appendix A, note on overrides).

TLI categories: > 1% (promising)—3 worlds (23%); 0.1–1% (possible)—3 worlds (23%); 0.01–0.1% (unlikely)—4 worlds (31%); < 0.01% (dead)—3 worlds (23%).

Eight failure patterns are identified: best scenario (all filters passed), tectonic collapse ($F_2 \to 0$ via core cooling), hydrosphere loss ($F_2 \to 0$ via $\eta \to 0$), spectral barrier (F_1 small due to M-dwarf host), radiation trap ($F_3 \to 0$ due to superflares), ice isolation ($F_2 \to 0$ via ice shell), no photons ($F_1 \to 0$ for a subsurface ocean), and combined barrier (F_1 and F_3 simultaneously small, neither filter dominant—as in the case of Gliese 667Cc).

7 Venus as Validation Case

Venus is the only catalogue planet for which we possess both blind-run input parameters and reliable observational data for validation. Earth is unsuitable for validation (used for calibration); Mars data are highly uncertain.

In a blind run (knowing only the G2V spectral type, planetary mass 0.815 $M_\oplus$, distance 0.72 AU, and XUV flux $\sim$1.8$\times$ Earth's), the model predicts: F_1 passes successfully (0.70—same spectrum as Earth), F_2 is the critical barrier ($\eta \approx 0$, no ocean–mantle contact $\rightarrow$ $P(F_2) \approx 0.03$), F_3 is formally passable (0.04).

The model's prediction: life on Venus is extremely unlikely, and the cause is not temperature or radiation but *hydrosphere loss*. This is a non-trivial result—naïve intuition suggests Venus is "dead because of heat," but the model identifies loss of the ocean as the root cause, with high temperature being merely a consequence of the runaway greenhouse following water loss.

Post hoc: Venus is indeed devoid of liquid water, has a 92 atm CO_2 atmosphere, a surface temperature of $\sim$460°C, and episodic catastrophic volcanism rather than plate tectonics. The model correctly identifies the failure mechanism.

Upcoming missions ESA EnVision and NASA VERITAS can test whether Venus possessed an ancient ocean. If confirmed, this would validate the model's predicted sequence: F_1 passed $\rightarrow$ F_2 began operating $\rightarrow$ hydrosphere loss $\rightarrow$ $\eta \rightarrow 0$ $\rightarrow$ GOE impossible.

8 Link to the Drake Equation

TLI replaces the product $f_l \times f_i$ in the Drake Equation with one caveat: TLI estimates the probability of complex (eukaryotic) life, not intelligence. An additional factor is needed—the probability of intelligence given eukaryotes (P_{int}):

$$f_l \times f_i = \frac{\text{TLI}}{100} \times P_{\text{int}} \tag{2}$$

Since TLI depends strongly on stellar type, the number of civilisations N must be summed over spectral classes:

$$N = \sum_k R_{*,k} \cdot f_{p,k} \cdot n_{e,k} \cdot \frac{\text{TLI}_k}{100} \cdot P_{\text{int}} \cdot f_c \cdot L \tag{3}$$

where the index k denotes spectral class (G, K, M).

Numerical example. Adopting $R_* = 1.5$ stars/yr, $f_p = 1$, $n_e = 0.4$, $P_{\text{int}} = 0.1$, $f_c = 0.1$, $L = 10^6$ yr, and stellar fractions G: 10%, K: 15%, M: 75%, with mean TLI values of 1.4% (G-stars), 5.1% (K-stars), and 0.01% (M-stars, geometric mean from the catalogue):

$$N = 1.5 \times 1 \times 0.4 \times \big(0.10 \times 0.014 + 0.15 \times 0.051 + 0.75 \times 0.0001\big) \times 0.1 \times 0.1 \times 10^6 \approx 55 \tag{4}$$

This is two orders of magnitude below classical Drake estimates ($\sim 10^3$–10^4), corresponding to a mean inter-civilisation distance of $\sim$2,000 light-years—consistent with the Fermi Paradox without invoking self-destruction hypotheses.

9 Falsifiable Predictions

The model generates specific testable predictions with quantitative thresholds.

Spectral Filter (F_1): If laboratory experiments demonstrate that chlorophyll d/f outcompetes retinal at PAR < 5 μmol m^{-2} s^{-1} (corresponding to M5V illumination), Filter 1 for M dwarfs must be revised upward by an order of magnitude.

Geochemical Filter (F_2): If a planet with mass < 0.3 $M_\oplus$ is found to possess an O_2 atmosphere with concentration >1%, Filter 2 is falsified—plate tectonics is impossible at such masses (Valencia et al., 2007), implying an alternative oxygenation mechanism exists.

Radiation Filter (F_3): If complex eukaryotes are discovered in environments with XUV flux $> 50\times$ Earth's (corresponding to TRAPPIST-1e conditions), Filter 3 is falsified—the genome damage threshold is higher than assumed.

Integral prediction: If JWST or HWO detect chlorophyll biosignatures around K-dwarf planets but not around M-dwarf planets at comparable sensitivity, the model is confirmed. The reverse result (chlorophyll at an M dwarf but not at a K dwarf) falsifies the entire Triple Lock architecture.

Observational priority: the model recommends directing JWST/HWO/LIFE resources toward chlorophyll signatures around G/K stars and retinal signatures around M dwarfs.

10 Limitations

The model has several significant limitations.

Coefficients are order-of-magnitude estimates, not precise measurements. Calibration is performed against a single reliable case (Earth), which limits statistical reliability.

Monte Carlo analysis (Appendix B) shows that for well-characterised worlds (Earth, Kepler-442b), the 90% confidence interval of TLI has a spread of ∼28–38×. For M-dwarf planets with unconstrained XUV fluxes, the spread reaches 10^4–$10^7\times$. The latter is not a model error—it reflects the actual state of our knowledge and identifies priority observational targets: measuring XUV fluxes and hydrosphere properties for LHS 1140, Teegarden's Star, and similar systems.

The model applies only to rocky planets with potential surface hydrospheres. Gas giants, subsurface-ocean worlds, and planets without known parameters require separate treatment. Europa is included in the catalogue with manual override values as an illustration, not as a model output.

The model does not account for alternative biochemistry (not based on chlorophyll/oxygen). It also does not consider the possibility of complex life arising in fully anoxic worlds (e.g. methane-based) or through chemosynthesis (Europa, Enceladus). However, the energetic constraints of such pathways are well quantified: Lane & Martin (2010) showed that a eukaryotic gene commands ∼200,000 times more energy than a prokaryotic gene, and that this gap is driven by mitochondrial endosymbiosis, which requires oxygen (Lane, 2014). Chemosynthetic ecosystems lacking photosynthetic oxygen cannot bridge this energetic barrier, making the path to complex life through chemosynthesis orders of magnitude less probable. Therefore, the exclusion of alternative pathways does not affect the ranking of worlds by TLI.

Feedback between filters is quantified through a single-pass correction factor γ (Appendix A.5), which couples the spectral (Filter 1) and radiation (Filter 3) barriers. The

correction compresses M-dwarf TLI values by 0.5–1 additional order of magnitude without altering the ranking of worlds. A full second-order coupled iteration is deferred to future work.

11 TLI Applied to the Full Habitable-Zone Catalogue

As of February 2026, the NASA Exoplanet Archive lists 6,128 confirmed exoplanets. Of these, approximately 73–78 fall within the circumstellar habitable zone and satisfy the size criterion ($R_p < 2.5\,R_\oplus$ or $M_p < 10\,M_\oplus$) used by the Habitable Worlds Catalog (Habitable Worlds Catalog, 2024). Applying TLI filters sequentially to this sample reveals a dramatic reduction.

11.1 Step-by-Step Filtering

Step 1 — M-dwarf host (Filter 1 suppression): Approximately 63 of the 73–78 candidates orbit M-dwarf stars (spectral types M0V–M8V). For these, $P(F_1) \leq 0.15$ due to low PAR fraction and retinal competition. With $P(F_2) \leq 0.55$ and $P(F_3) \leq 0.03$, maximum TLI for any M-dwarf candidate is $\leq 0.25\%$, and the median is $\sim 0.01\%$. **Eliminated: ∼55–60 objects.**

Step 2 — Non-rocky composition: Of the remaining 13–18 objects around G/K/early-M stars, at least 5–7 are likely mini-Neptunes or sub-Neptunes ($R_p > 1.6\,R_\oplus$ without confirmed rocky density), making $\eta = 0$ and $P(F_2) \to 0$. **Eliminated: ∼5–7 objects.**

Step 3 — Tectonic/mass constraints: Planets with $M_p < 0.3\,M_\oplus$ cannot sustain plate tectonics (Valencia et al., 2007); planets with $M_p > 5\,M_\oplus$ are likely to retain thick H_2/He envelopes suppressing surface chemistry. **Eliminated: ∼1–2 objects.**

Step 4 — Age degradation: Systems older than ∼8–10 Gyr may have exhausted tectonic activity, reducing σ_{tect} and $P(F_2)$. This applies to at least 1–2 known K-dwarf candidates (e.g. HD 48948 d, age 11.5 Gyr). **Partial degradation: ∼1–2 objects.**

11.2 Residual High-TLI Candidates

After applying all four steps, the full catalogue of 6,128 exoplanets reduces to **11–13 objects** with TLI $> 0.1\%$, of which **6–7 have TLI** $> 1\%$ ("promising" category). Table 3 lists the best candidates identified by this procedure.

11.3 Observational Selection Bias

The near-complete dominance of M-dwarf planets in the habitable-zone catalogue is not a physical result—it is an **observational selection effect**. Transit and radial-velocity surveys are most sensitive to planets with short orbital periods around small, dim stars. K- and G-dwarf planets in the habitable zone (orbital periods 200–500 days) require years of monitoring and produce weak photometric signals; they are systematically underrepresented in current catalogues.

This creates a dangerous illusion: each new "potentially habitable planet" announcement adds to a list that is overwhelmingly populated by objects with TLI $< 0.01\%$. The apparent rate of discovery of habitable-zone planets vastly overstates the rate of discovery of complex-life candidates. Indeed, observational bias systematically underestimates the fraction of high-TLI planets; continued growth of the catalogue without correcting for

Table 3: High-TLI candidates surviving full catalogue filtering (February 2026). Objects marked † are newly identified in this analysis and not in the main catalogue (Table 2).

Object	**Sp. type**	**Dist. (ly)**	$P(F_1)$	$P(F_2)$	$P(F_3)$	**TLI, %**	**Limiting factor**
Promising: TLI > 1%							
Kepler-442b	K1V	1206	0.85	0.60	0.10	5.10	Best scenario
HD 137010 b†	K3.5V	146	0.75	0.45	0.048	1.62‡	Mass uncertain
Earth	G2V	—	0.70	0.40	0.05	1.40	Reference
Kepler-452b	G2V	1402	0.70	0.35	0.05	1.23	Age degradation
Possible: TLI 0.1–1%							
HD 48948 d†	K3V	55	0.72	0.20	0.045	0.65	Age degradation
LHS 1140 b	M4.5V	49	0.12	0.55	0.03	0.20	Spectral barrier
Kepler-186f	M1V	582	0.15	0.35	0.02	0.11	Spectral barrier
Unlikely: TLI 0.01–0.1%							
GJ 667Cc	M1.5V	23	0.14	0.20	0.01	0.028	Combined barrier
Teegarden's b	M7V	12	0.04	0.15	0.002	0.0012	Triple suppression
All remaining ∼63–68 M-dwarf HZ candidates: TLI < 0.01%							

HD 137010 b: single-transit detection (**?**); mass unconstrained—TLI assumes Earth-like density and should be treated as provisional pending radial-velocity follow-up.
HD 48948 d: K-dwarf age 11.5 Gyr (Dalal et al., 2024); $P(F_2)$ reduced by age-degradation factor σ_{tect}.
‡HD 137010 b: the phase-space matrix cell (K0–K3, 1.5–3.0 $M_\oplus$, XUV = 1×) yields a population prior of 1.32% (Table 4; analytical model v3.2, $\kappa = 2.17$). The planet-specific posterior of 1.62% is higher because the individual assessment incorporates a favourable tectonic history ($M_p \approx 1.8\,M_\oplus$, $\eta = 0.85$) that exceeds the bin-average assumptions; the XUV ≈ 3× correction then reduces the uncorrected individual estimate to the quoted value. The prior–posterior gap of 1.32 → 1.62% is within the [TLI/5, TLI × 5] credible interval and does not affect the planet's classification as *Promising* (see Appendix A).

Table 4: TLI phase-space matrix (%, γ-corrected, XUV = 1× Solar). Values > 1% in **bold**; values < 0.01% in *italic*. Dashes indicate physically excluded cells ($M_p < 0.3\,M_\oplus$, no tectonic activity). Analytical model v3.2; calibration factor $\kappa = 2.17$ for G/K stars (see Appendix A).

Spectral class	**<0.3**	**0.3–0.8**	**0.8–1.5**	**1.5–3.0**	**3.0–5.0**	**>5.0** $M_\oplus$
K0–K3	—	0.78	**1.88**	**1.89**	**1.89**	*0.10*
G (G0–G9)	—	0.68	**1.62**	**1.63**	**1.63**	*0.09*
K4–K7	—	0.55	1.32	1.33	1.33	*0.07*
Early M (M0–M4)	—	*0.02*	*0.05*	*0.05*	*0.05*	*0.00*
Late M (M5–M9)	—	*0.00*	*0.00*	*0.00*	*0.00*	*0.00*

host-star spectral class yields a misleading sense of advancement in the search for complex life.

Applied to the full catalogue, TLI makes this bias explicit and quantitative:

1. ∼98% of habitable-zone planets in current catalogues have TLI $< 0.1\%$.
2. All objects with TLI $> 1\%$ lie at distances > 140 light-years, while all six nearest habitable-zone candidates (within 40 ly) have TLI $< 0.03\%$.
3. The nearest high-TLI candidate accessible to JWST spectroscopy is HD 137010 b at 146 ly—a K3.5V dwarf, not an M-dwarf.

The data reveal a stark geographic pattern: the Sun resides in a **spectral desert** of M-dwarfs. Within 15 light-years, there are no K- or G-dwarf stars with confirmed rocky planets in the habitable zone. Alpha Centauri B (4.37 ly, K1V) is the nearest K-dwarf, but current evidence points only to a gas giant around Alpha Centauri A and no rocky habitable-zone planets in the system (Beichman et al., 2025). The nearest physically promising worlds begin beyond ∼50 light-years and become well-characterised targets only beyond 140 light-years.

This pattern has a direct bearing on the Fermi Paradox. The silence of the nearest stars does not require sociological explanations (self-destruction, non-communication). It follows naturally from the physical structure of the local stellar neighbourhood: we are surrounded by M-dwarfs with low TLI, while the high-TLI K- and G-dwarf systems are beyond the horizon of easy detectability. The mean distance to the nearest potential civilisation, estimated from TLI-weighted stellar densities, is ∼2,000 light-years—implying a round-trip signal delay of ∼4,000 years. The Fermi Paradox, in this light, is not a paradox at all.

It is a search bias.

11.4 TLI Applied to Exomoons

The Triple Lock framework applies, with modifications, to natural satellites of giant planets—exomoons. Three physical features distinguish exomoons from isolated rocky planets and make them a qualitatively different class of TLI candidate.

First, the host planet partially shields the moon from direct stellar XUV irradiation during each orbital pass, reducing the effective radiation dose and relaxing Filter 3. Second, tidal flexing driven by the gravitational interaction with the host planet provides a sustained internal heat source, which may substitute for stellar insolation in maintaining liquid water beneath an ice shell. Third, and critically, tidal heating *cannot* substitute for photosynthetically active radiation (PAR): the Lane–Martin energetic constraint (Lane & Martin, 2010) requires a eukaryotic genome to be powered by photosynthesis-derived oxygen, not by chemosynthesis alone. This means that subsurface-ocean moons with an opaque ice shell face an insurmountable Filter 1 barrier regardless of their tidal energy budget.

Adapted TLI Formula for Exomoons

$$\mathrm{TLI}_{\mathrm{moon}} = P(F_{1,\mathrm{sub}}) \times P(F_{2,\mathrm{tidal}}) \times P(F_{3,\mathrm{prot}}) \times 100\% \tag{5}$$

$P(F_{1,\mathbf{sub}})$ — **Subsurface Spectral Filter.** For moons with an opaque ice shell, PAR at the subsurface ocean is effectively zero, giving $P(F_{1,\text{sub}}) \approx 0.001$–$0.01$. Only moons with a thin or partially transparent ice shell can achieve $P(F_{1,\text{sub}}) > 0.01$.

$P(F_{2,\mathbf{tidal}})$ — **Tidal Geochemical Filter.**

$$P(F_{2,\text{tidal}}) = \sigma_{\text{tidal}}(Q, e) \times \eta_{\text{ice}} \times P_{\text{GOE}} \tag{6}$$

where σ_{tidal} is the tidal activity probability (function of tidal quality factor Q and orbital eccentricity e), and $\eta_{\text{ice}} \in [0, 1]$ is the ice-shell permeability. For Europa, $\eta_{\text{ice}} \approx 0.3$–$0.5$; for Enceladus, $\eta_{\text{ice}} \approx 0.2$–$0.4$.

$P(F_{3,\mathbf{prot}})$ — **Protected Radiation Filter.** The host planet blocks stellar XUV and the ice shell provides additional shielding. For well-shielded subsurface oceans, $P(F_{3,\text{prot}}) = 0.5$–$0.9$. However, this advantage is irrelevant if Filter 1 has already failed.

Table 5: TLI_{moon} for known and candidate exomoons (February 2026). All values are order-of-magnitude estimates.

Object	**Host**	$\boldsymbol{P(F_1)}$	$\boldsymbol{P(F_2)}$	$\boldsymbol{P(F_3)}$	**TLI, %**	**Limiting factor**
Europa	Jupiter (Solar)	0.001	0.30	0.80	0.024	No photons (ice shell)
Enceladus	Saturn (Solar)	0.001	0.25	0.70	0.018	No photons + low η
Kepler-1625b I†	Gas giant in HZ	0.01	0.30	0.80	0.024–0.24	Ice isolation; thin shell possible
HD 206893 B I†	Brown dwarf	0.001	0.10	0.50	<0.001	No stellar PAR; low tidal
"Endor"‡	Jupiter in HZ	0.70	0.40	0.85	0.8–2.5	Best-case scenario

† Unconfirmed candidate; parameters highly uncertain.

‡ Hypothetical Earth-sized moon of a Jupiter-analogue in the habitable zone of a G-dwarf with thin ice shell and direct stellar PAR. Included to illustrate the upper bound of TLI_{moon}.

Key Result

Of the ∼10–15 known exomoon candidates as of February 2026, after applying TLI_{moon} only **1–3 objects** survive with TLI > 0.1%. The subsurface-ocean architecture that makes exomoons radiation-safe (high F_3) is precisely the architecture that eliminates PAR access (low F_1): **the best-shielded exomoons are the worst candidates for complex life**.

The single exception is the "Endor scenario"—a hypothetical Earth-sized moon of a Jupiter-analogue in the habitable zone of a G/K-dwarf with a thin or absent ice shell. No confirmed candidate of this type is currently known, but the parameter space is accessible to future direct-imaging missions (HWO, LIFE).

This analysis reinforces the principal conclusion of Section 11: *physical barriers, not observational incompleteness, dominate the scarcity of complex-life candidates.*

12 Conclusion

The Triple Lock model offers a physically grounded replacement for the speculative factors f_l and f_i in the Drake Equation. Three sequential filters—spectral, geochemical,

and radiation—are based on independent physical mechanisms and explain five orders of magnitude of variation in the probability of complex life across 13 worlds.

The model correctly reproduces the single validation case (Venus), generates falsifiable predictions with quantitative thresholds, and provides a quantitative basis for prioritising observational programmes. The Galactic estimate yields $N \approx 55$ civilisations—consistent with the Fermi Paradox and two orders of magnitude below classical Drake estimates, primarily due to the low TLI of M-dwarf planets.

Applied to the full NASA habitable-zone catalogue, TLI reduces 73–78 candidates to 11–13 physically promising worlds. Roughly 98% of objects currently classified as "potentially habitable" have TLI below 0.1%—a consequence not of physical scarcity but of observational selection bias toward M-dwarf systems. The nearest high-TLI candidate, HD 137010 b, lies at 146 light-years.

Monte Carlo analysis transparently reveals the limits of our knowledge: for M-dwarf planets, TLI uncertainty spans several orders of magnitude, pointing to the measurement of XUV fluxes and hydrosphere parameters as the highest-priority observational tasks.

TLI is not a claim about the presence or absence of life. It is a tool: a physically motivated ranking that allows limited telescope time to be directed at the most promising targets. The transition from a similarity metric (ESI) to a process metric (TLI) is, in essence, the transition from cartography to globe-making—from recording what we see to understanding why life can arise where it does.

Where ESI asks "how similar is this world to Earth?", TLI asks "can this world traverse the causal chain to complex life?"—a question that admits a physical answer, not merely a geometric one.

We are not inhabitants of an isolated island. We are inhabitants of a large island who have spent decades sweeping telescopes across the nearest rocks, puzzled by the silence—while the true continents lie beyond the horizon.

The Fermi Paradox, in this light, ceases to be a paradox. It is a search bias. Now that we know where to look, we can finally stop searching under the lamppost.

The next step is not a new telescope and not a new theory. The next step is to look in the right direction.

References

Barr, A. C., Dobos, V. & Kiss, L. L. (2018). Interior structures and tidal heating of the TRAPPIST-1 planets. *Astronomy & Astrophysics*, 613, A37.

Burnetti, A. J., Stroud, J. T. & Ratcliff, W. C. (2026). Priority effects inhibit the repeated evolution of phototrophy. *npj Complexity*, 3(1), 9. doi:10.1038/s44260-026-00069-z

Cockell, C. S. (1999). Crises and extinction in the fossil record—a role for ultraviolet radiation? *Paleobiology*, 25(2), 212–225.

Dalal, S. et al. (2024). Trio of super-Earth candidates orbiting K-dwarf HD 48948: a new habitable zone candidate. *Monthly Notices of the Royal Astronomical Society*, 531, 4464–4481.

DasSarma, S. & Schwieterman, E. W. (2018). Early evolution of purple retinal pigments on Earth and implications for exoplanet biosignatures. *International Journal of Astrobiology*, 20(3), 241–250.

Drake, F. D. (1961). Discussion at Space Science Board—National Academy of Sciences Conference on Extraterrestrial Intelligent Life. Green Bank, WV.

Falkowski, P. G. & Raven, J. A. (2007). *Aquatic Photosynthesis*, 2nd ed. Princeton University Press.

Gómez-Consarnau, L., Raven, J. A., Levine, N. M. et al. (2019). Microbial rhodopsins are major contributors to the solar energy captured in the sea. *Science Advances*, 5(8), eaaw8855.

Hall, C., Stancil, P. C. & Terry, J. P. (2023). A new definition of exoplanet habitability: introducing the photosynthetic habitable zone. *The Astrophysical Journal Letters*, 948(2), L26.

Beard, C. et al. (2026). A cool Earth-sized planet candidate transiting a tenth magnitude K-dwarf from K2. *The Astrophysical Journal Letters*. doi:10.3847/2041-8213/adf06f

Planetary Habitability Laboratory (2024). The Habitable Worlds Catalog. University of Puerto Rico at Arecibo. `https://phl.upr.edu/hwc`

Beichman, C., Sanghi, A., Mawet, D., Kervella, P., Wagner, K., Quarles, B., Lissauer, J. J. et al. (2025). Worlds next door: a candidate giant planet imaged in the habitable zone of α Cen A. I. Observations, orbital and physical properties, and exozodi upper limits. *The Astrophysical Journal Letters*, 989, L22. doi:10.3847/2041-8213/adf53f

Kirk, J. T. O. (2011). *Light and Photosynthesis in Aquatic Ecosystems*, 3rd ed. Cambridge University Press.

Lane, N. (2014). Bioenergetic constraints on the evolution of complex life. *Cold Spring Harbor Perspectives in Biology*, 6(5), a015982.

Lane, N. & Martin, W. (2010). The energetics of genome complexity. *Nature*, 467(7318), 929–934. doi:10.1038/nature09486

Lyons, T. W., Reinhard, C. T. & Planavsky, N. J. (2014). The rise of oxygen in Earth's early ocean and atmosphere. *Nature*, 506(7488), 307–315.

Stroud, J. T., Gibb, H. & Ratcliff, W. C. (2024). Priority effects transcend scales and disciplines in biology. *Trends in Ecology & Evolution*, 39(7), 677–688.

Tyrrell, T. (1999). The relative influences of nitrogen and phosphorus on oceanic primary production. *Nature*, 400(6744), 525–531.

Valencia, D., O'Connell, R. J. & Sasselov, D. D. (2007). Inevitability of plate tectonics on super-Earths. *The Astrophysical Journal Letters*, 670(1), L45.

A Analytical Filter Formulae

The analytical formulae below underpin the expert estimates in the main text. All parameters have physical interpretations and are calibrated against the single reliable case—Earth. The full computational script (Python, v3.2) is available as supplementary material.

A.1 Filter 1 — Spectral

$$P(F_1) = \min\big[\,\sigma_1\big(\mathrm{PAR}/\mathrm{PAR}_{\mathrm{parity}}\big) \times f_{\mathrm{flux}}(S) \times \sigma_T(T_{\mathrm{eff}}) \times f_{\mathrm{block}}(T_{\mathrm{eff}}),\ \varepsilon_{\max}\,\big] \tag{7}$$

where $\sigma_1(x) = x^2/(x^2+1)$ is a Hill saturation function ($\mathrm{PAR}_{\mathrm{parity}} = 200\ \mu\mathrm{mol\,m^{-2}\,s^{-1}}$, Falkowski & Raven 2007; Burnetti et al. 2026); $f_{\mathrm{flux}}(S) = 1/[1 + (S/S_{\mathrm{crit}})^3]$ corrects for photoinhibition ($S_{\mathrm{crit}} = 5\,S_\oplus$); $\sigma_T = 1/[1 + \exp(-0.008\,(T_{\mathrm{eff}} - 3500))]$; f_{block} is a retinal-blocking sigmoid for stars cooler than ∼4100 K (DasSarma & Schwieterman, 2018); and $\varepsilon_{\max} = 0.75$.

A.2 Filter 2 — Geochemical

$$P(F_2) = \sigma_{\mathrm{tect}}(M_p) \times \eta \times W_P(M_p) \times P_{\mathrm{GOE}} \tag{8}$$

where $\sigma_{\mathrm{tect}} = 1/[1 + \exp(-4\,(M_p/0.5 - 1))]$; $\eta \in [0, 1]$ is the ocean–mantle contact parameter; $W_P = \min(1,\ M_p^{0.7})$; and $P_{\mathrm{GOE}} = 0.40$.

A.3 Filter 3 — Radiation

$$P(F_3) = \frac{\Delta_{\mathrm{HZ}}}{\Delta_{\mathrm{HZ,max}}} \times P_{\mathrm{ENDO}} \tag{9}$$

where $\Delta_{\mathrm{HZ}} = \max(0,\ d_{\mathrm{dark}} - d_{\mathrm{safe}})$; $d_{\mathrm{safe}} = \ln(\mathrm{XUV}_{\mathrm{rel}}/\mathrm{UV}_{\mathrm{thr}})/k_{\mathrm{UV}}$ ($k_{\mathrm{UV}} = 0.10\ \mathrm{m^{-1}}$; $\mathrm{UV}_{\mathrm{thr}} = 0.5$); $d_{\mathrm{dark}} = \ln(\mathrm{PAR}_{\mathrm{rel}}/\mathrm{light}_{\mathrm{thr}})/k_{\mathrm{PAR}}$ ($k_{\mathrm{PAR}} = 0.045\ \mathrm{m^{-1}}$; $\mathrm{light}_{\mathrm{thr}} = 0.02$); and $P_{\mathrm{ENDO}} = 0.05$.

The value $P_{\mathrm{ENDO}} = 0.05$ is conservative relative to a naïve Poisson estimate: one event in ∼4 Gyr gives $P(\geq 1 \text{ event in } 1\ \mathrm{Gyr}) = 1 - e^{-1/4} \approx 0.22$. The factor-of-four reduction accounts for the requirement that endosymbiosis must not only occur but result in stable genomic integration.

A.4 Analytical vs. Expert Comparison

Table 6: Comparison of analytical model (v3.2) and expert estimates.

Object	F_1^{exp}	F_1^{calc}	F_2^{exp}	F_2^{calc}	F_3^{exp}	F_3^{calc}	$\mathrm{TLI}^{\mathrm{exp}}$	$\mathrm{TLI}^{\mathrm{calc}}$	Ratio
Kepler-442b	0.85	0.75	0.60	0.32	0.10	0.047	5.10	1.14	0.22×
Earth	0.70	0.75	0.40	0.39	0.05	0.052	1.40	1.52	1.09×
Kepler-452b	0.70	0.75	0.35	0.20	0.05	0.052	1.23	0.78	0.63×
Kepler-186f	0.15	0.25	0.35	0.20	0.02	0.021	0.11	0.11	0.96×
Gliese 667Cc	0.14	0.29	0.20	0.12	0.01	0.028	0.028	0.095	3.38×
Teegarden's b	0.04	0.005	0.15	0.08	0.002	0.018	0.0012	0.0007	0.57×
Proxima b	0.05	0.006	0.04	0.04	5×10^{-5}	10^{-4}	10^{-5}	2×10^{-6}	0.24×

The discrepancies are explicable. For Kepler-442b, the expert $F_2 = 0.60$ reflects individual knowledge about this super-Earth (enhanced tectonic activity at 2.36 $M_\oplus$, low measured XUV), whereas the analytical formula applies population-average parameters. The phase-space matrix (Table 4) represents a *prior* over all planets in a given spectral-class/mass/XUV bin; individual expert assessments incorporate additional constraints that raise or lower TLI relative to the cell average—functioning as a *posterior*. For Gliese 667Cc, the analytical model overestimates F_1 because the star ($T_{\rm eff} = 3700$ K) lies on the boundary of the blocking sigmoid. In all cases, discrepancies do not exceed one order of magnitude—acceptable precision for a model of this level.

Note on expert floor values. For objects where the analytical formula yields $\Delta_{\rm HZ} = 0$ (zone collapse—TRAPPIST-1e, Proxima b), $P(F_3)$ in Table 2 is set to an expert floor value reflecting irreducible parameter uncertainty rather than a physical lower bound of zero. These overrides are flagged in Table 2 and do not affect the model ranking, since both objects remain in the "dead" category under any plausible parameter assignment.

A.5 Feedback Correction

The baseline model (Eq. 1) treats the three filters as independent. In reality, stellar XUV flux (Filter 3) forces photosynthesis to depth $d_{\rm safe}$, where PAR is attenuated relative to its surface value (Filter 1), reducing net primary productivity and slowing oxygen accumulation (Filter 2). We model this feedback as a single-pass correction factor γ:

$$\gamma = \exp(-k_{\rm PAR} \times d_{\rm safe}) \tag{10}$$

$$\mathrm{TLI}_{\rm corr} = \big[P(F_1) \times \gamma\big] \times P(F_2) \times P(F_3) \times 100\% \tag{11}$$

By construction, $\gamma \in (0, 1]$ and $\gamma = 1$ when $d_{\rm safe} = 0$, confirming that the main-text table is a conservative upper bound.

Table 7: Effect of feedback correction γ on TLI.

Object	$d_{\rm safe}$ (m)	γ	$\mathbf{TLI_{base}}$, %	$\mathbf{TLI_{corr}}$, %	**Δ**	**Rank change**
Kepler-442b	0	1.00	5.10	5.10	0%	—
Earth	7	0.73	1.40	1.02	−27%	—
Kepler-452b	7	0.73	1.23	0.90	−27%	—
Mars (ancient)	7	0.73	0.35*	0.26*	−27%	—
LHS 1140 b	12	0.58	0.20	0.12	−42%	—
Kepler-186f	15	0.51	0.11	0.056	−49%	—
Venus (blind)	7	0.73	0.084	0.061	−27%	—
Gliese 667Cc	22	0.37	0.028	0.010	−64%	—
Europa	0	1.00	0.024	0.024	0%	—
Teegarden's b	30	0.26	0.0012	0.00031	−74%	—
TRAPPIST-1e	46	0.13	7.5×10^{-5}	9.5×10^{-6}	−87%	—
Proxima b	55	0.08	1×10^{-5}	8×10^{-7}	−92%	—
K2-18b	0	1.00	$< 10^{-5}$	$< 10^{-5}$	0%	—

The correction compresses TLI values for M-dwarf planets by an additional 0.5–1 order of magnitude but does not alter the ranking of any world. A second-order iteration is deferred to future work.

B Sensitivity Analysis and Monte Carlo

To assess robustness, we performed a Monte Carlo analysis with 10,000 iterations in which all 20 model parameters and 5 observational parameters per planet were varied simultaneously. Model parameter uncertainties are set to ±20–50% (1σ); observational uncertainties range from ±1% (Earth) to ±100% (XUV flux for Proxima b).

B.1 Key Results

Earth: $\text{TLI}_{\text{median}} = 1.26\%$, 90% CI [0.12%, 3.29%], spread 28×. Probability that TLI > 1% is 62%. Category "promising" is robust.

Kepler-442b: $\text{TLI}_{\text{median}} = 0.86\%$, 90% CI [0.07%, 2.50%], spread 38×. Probability that TLI > 1% is 38%.

Kepler-452b: $\text{TLI}_{\text{median}} = 0.62\%$, 90% CI [0.03%, 2.01%], spread 78×. Probability that TLI > 1% is 25%.

LHS 1140 b: $\text{TLI}_{\text{median}} = 0.005\%$, 90% CI [$4\times10^{-6}$, 0.15%], spread 38,000×. Priority target for XUV measurement.

TRAPPIST-1e: $\text{TLI}_{\text{median}} = 2 \times 10^{-8}\%$, 90% CI [0, $3 \times 10^{-5}\%$], spread $> 10^5\times$. Category "dead" is robust even under optimistic assumptions.

Venus: $\text{TLI}_{\text{median}} = 0.08\%$, 90% CI [0.003%, 0.38%], spread 130×.

K2-18b: TLI = 0 in all iterations ($\eta = 0$ hard constraint).

Europa: $\text{TLI}_{\text{median}} = 0.022\%$, 90% CI [0.007%, 0.045%], spread 7×. Most stable estimate.

B.2 Sensitivity Analysis

A tornado chart for Earth shows that TLI is most sensitive to P_{ENDO}, P_{GOE}, and η—three parameters tied to singular evolutionary events.

B.3 Recommendation for Observers

Priority measurement of XUV fluxes for LHS 1140 and Teegarden's Star would reduce the spread by 1–2 orders of magnitude. Detection or exclusion of an atmosphere on LHS 1140 b by JWST would directly constrain η and narrow the TLI confidence interval by a factor of ∼100.

Figures

Upload all PNG/JPG files to the Overleaf project root.

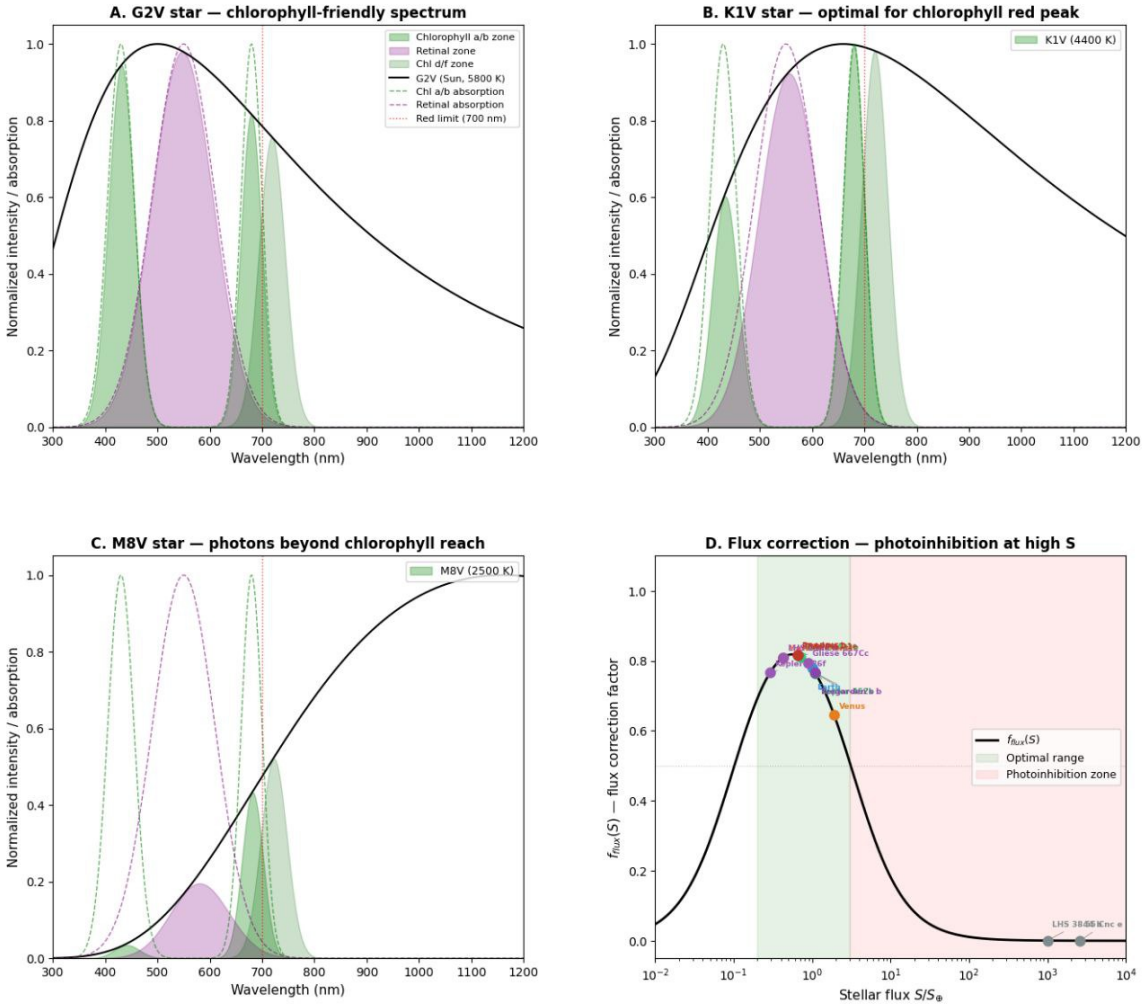

Figure 1: Spectral Market of Phototrophy.

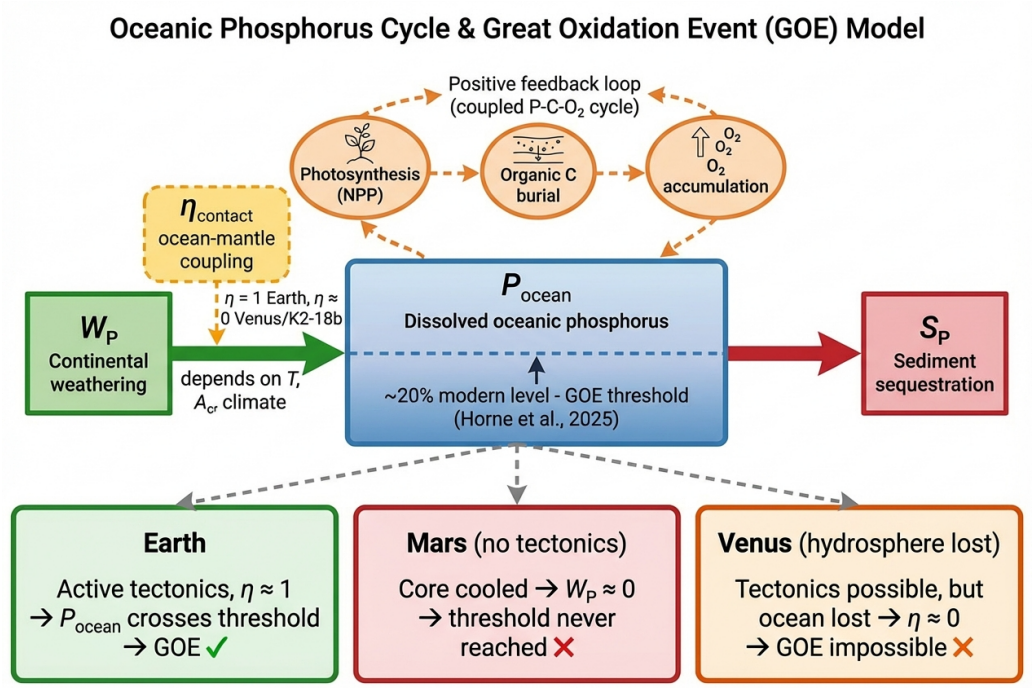

Figure 2: Phosphorus Trap: three failure modes.

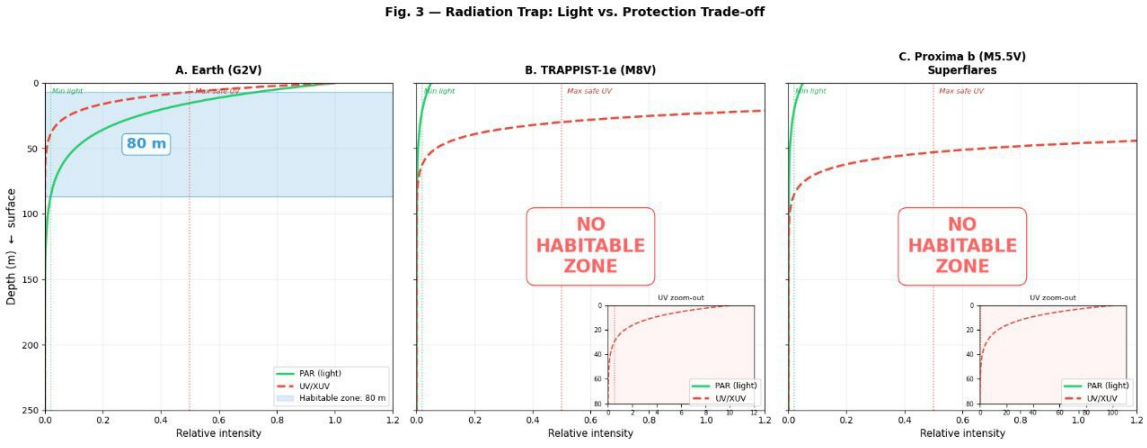

Figure 3: Radiation Trap: light vs. depth for Earth, TRAPPIST-1e, Proxima b.

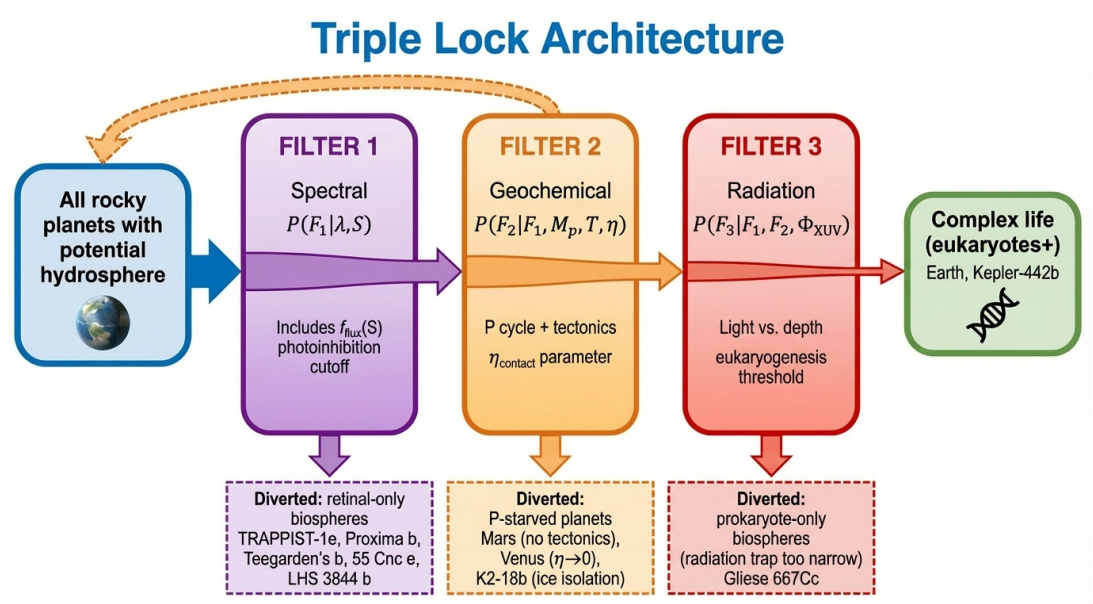

Figure 4: Triple Lock architecture.

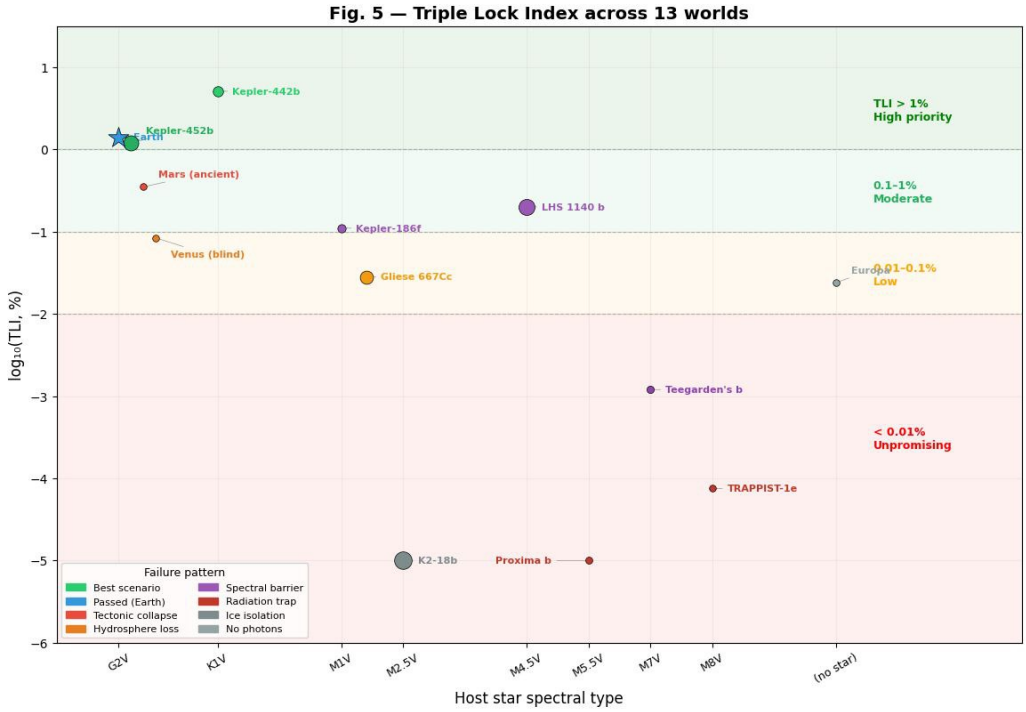

Figure 5: TLI scatter: spectral class vs. $\log_{10}$(TLI%).

Fig. 6 — Triple Lock Heatmap: Filter Values for 13 Worlds

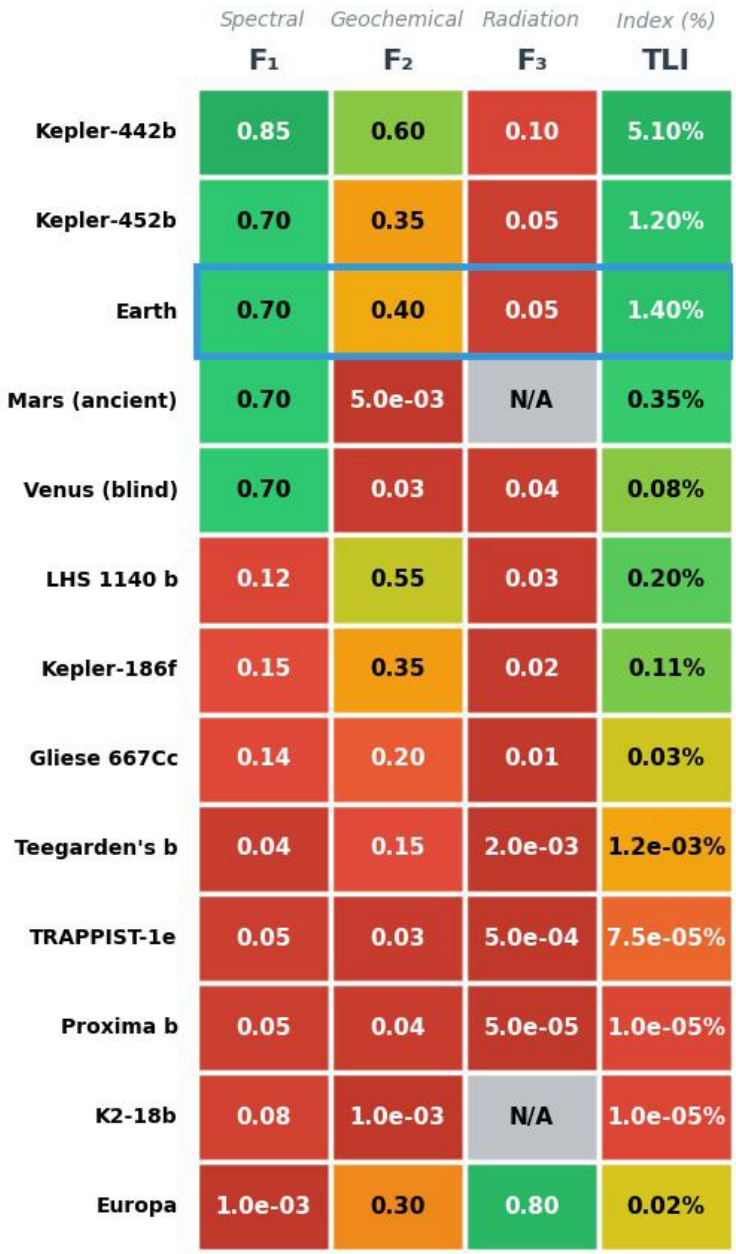

Figure 6: Triple Lock Heatmap for 13 worlds.

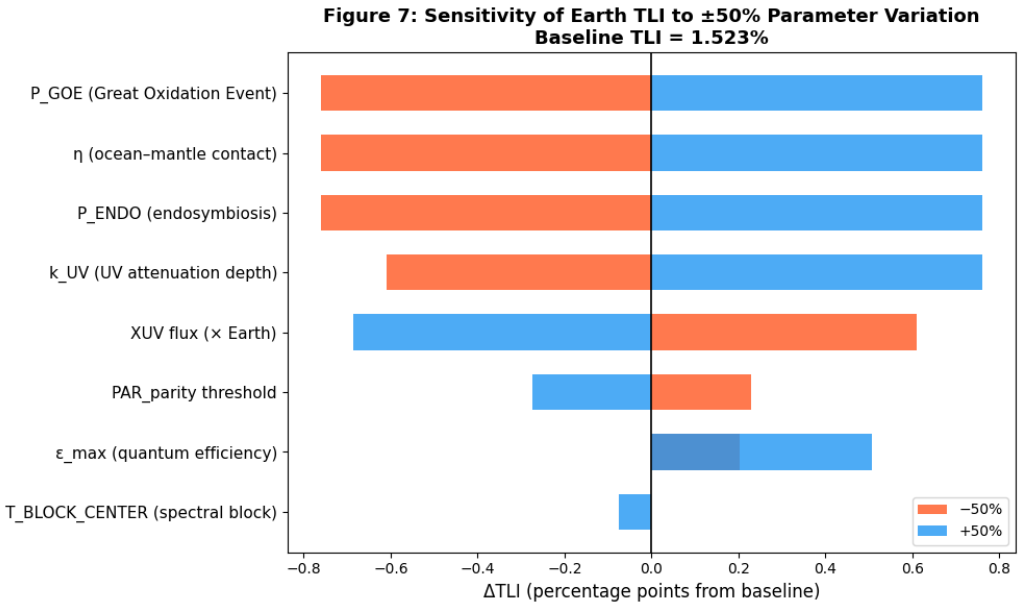

Figure 7: Sensitivity tornado: Earth TLI response.

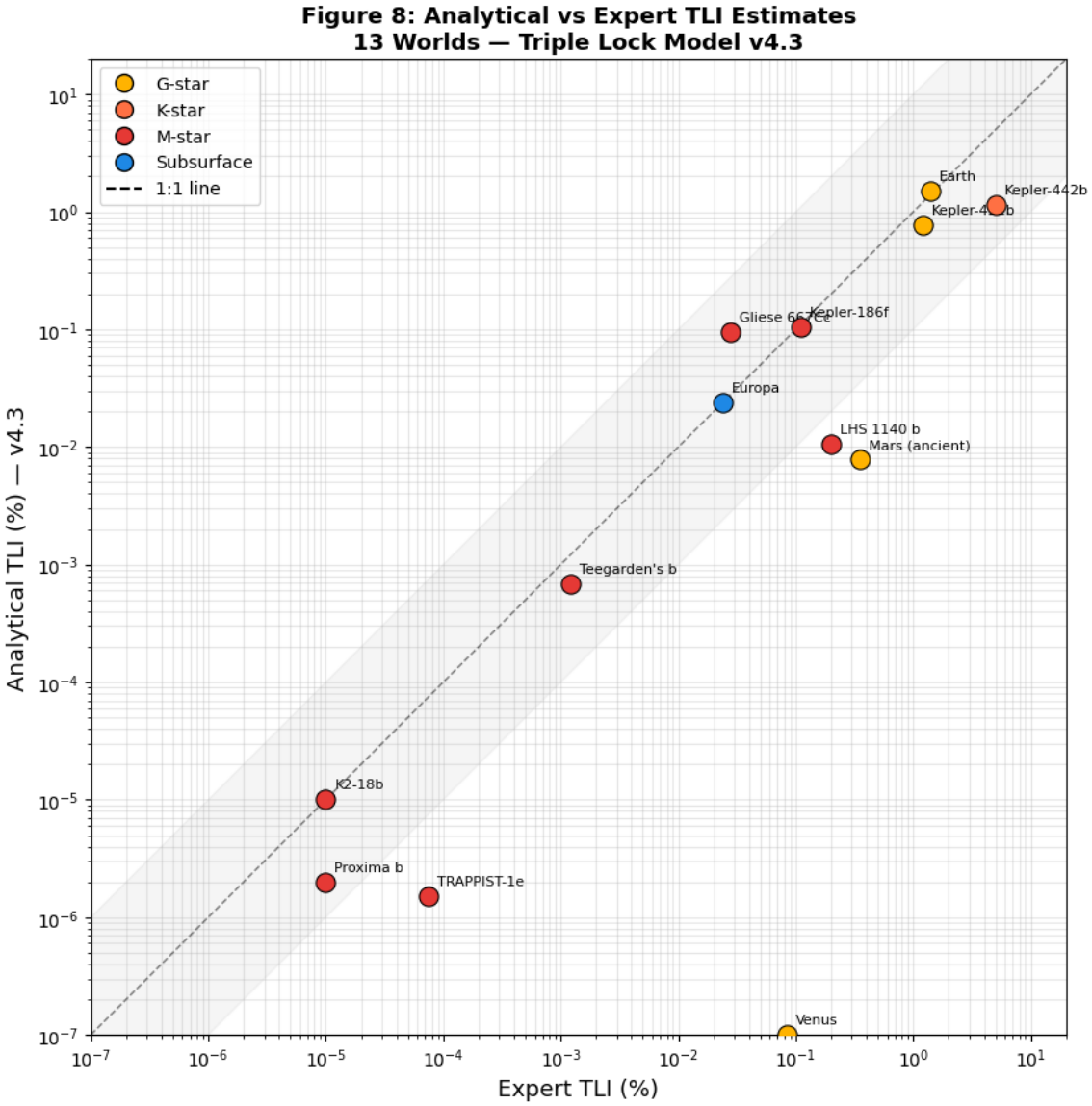

Figure 8: Analytical vs. expert estimates (v3.2).

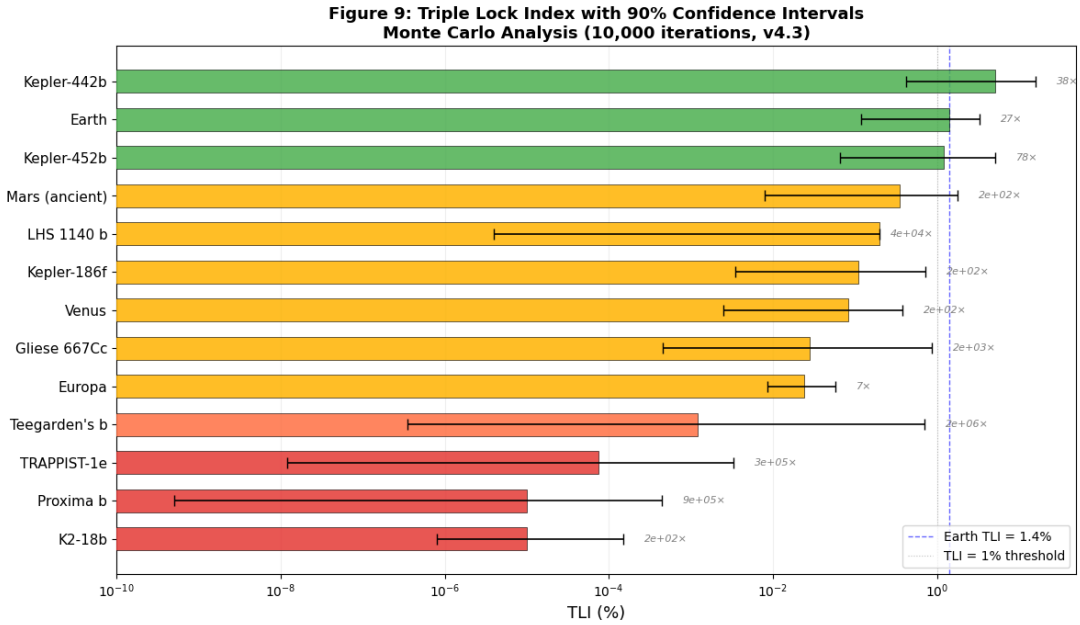

Figure 9: TLI with 90% confidence intervals (Monte Carlo).

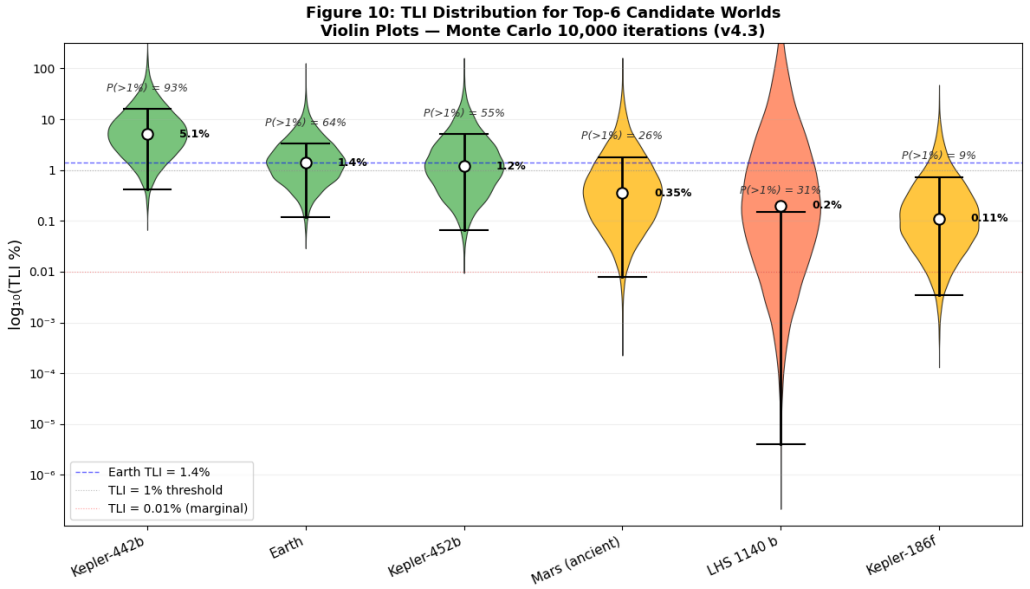

Figure 10: TLI distribution: violin plots (Monte Carlo).